

Three dimensional characterization of tissue-engineered constructs by contrast enhanced nanofocus computed tomography

Ioannis Papantoniou, PhD^{1,3*}, Maarten Sonnaert^{1, 2*}, Liesbet Geris, Prof.^{1,4,5}, Frank P. Luyten, Prof.^{1,3}, Jan Schrooten, PhD^{1,2}, Greet Kerckhofs, PhD^{1,2,5}

¹Prometheus, Division of Skeletal Tissue Engineering, KU Leuven, Onderwijs en Navorsing 1 (+8), Herestraat 49 - PB813, B-3000 Leuven, Belgium.

²Department of Metallurgy and Materials Engineering, KU Leuven, Kasteelpark Arenberg 44 – PB 2450, B-3001 Heverlee, Belgium.

³Cell and Gene Therapy Applications, KU Leuven, Onderwijs en Navorsing 1 (+8), Herestraat 49 - PB813, B-3000 Leuven, Belgium.

⁴Department of Mechanical Engineering - Biomechanics Section, KU Leuven, Celestijnenlaan 300 C - PB 2419, B-3001 Heverlee, Belgium.

⁵Biomechanics Research Unit, Université de Liege, Chemin des Chevreuils 1 - BAT 52/3, B-4000 Liège, Belgium.

Dr. Ioannis Papantoniou* : ioannis.papantoniou@med.kuleuven.be; tel. : 0032 16 346166

Maarten Sonnaert* : maarten.sonnaert@mtm.kuleuven.be; tel. : 0032 16 346142

Prof. Liesbet Geris : liesbet.geris@ulg.ac.be; tel. : 0032 4 3669587

Prof. Frank P. Luyten : frank.luyten@uz.kuleuven.ac.be; tel. : 0032 16 342541

Dr. Jan Schrooten : jan.schrooten@mtm.kuleuven.be; tel. : 0032 16 321212

Dr. Greet Kerckhofs : greet.kerckhofs@mtm.kuleuven.be; tel. : 0032 16 346189

*These authors have contributed equally and therefore share first authorship

Abstract

In order to successfully implement tissue engineered (TE) constructs as part of a clinical therapy, it is necessary to develop quality control tools that will ensure accurate and consistent TE construct release specifications. Hence advanced methods to monitor TE construct properties need to be further developed. In this study we showed proof of concept for contrast enhanced nanofocus computed tomography (CE-nanoCT) as a ‘whole-construct’ imaging technique with non-invasive potential that enables 3D visualization and quantification of *in vitro* engineered extracellular matrix (ECM) in TE constructs. In particular we performed a 3D qualitative and quantitative structural and spatial assessment of the *in vitro* engineered ECM, formed during static and perfusion bioreactor cell culture in 3D TE scaffolds, using two contrast agents, namely Hexabrix[®] and phosphotungstic acid (PTA). To evaluate the potential of CE-nanoCT, a comparison was made to standardly used techniques such as Live/Dead viability/cytotoxicity, picrosirius red staining and to net dry weight measurements of the TE constructs. When using Hexabrix[®] as contrast agent, the ECM volume fitted linearly with net dry ECM weight independent from the flow rate used, hence suggesting that it stains most of the ECM. When using PTA as contrast agent, comparing to net weight measurements showed that PTA only stains a part of the ECM. This was attributed to the binding specificity of this contrast agent. Also, the PTA-stained CE-nanoCT data showed pronounced distinction between flow conditions when compared to Hexabrix[®], indicating culture-specific structural ECM differences. This novel type of information can contribute to optimize bioreactor culture conditions and potentially critical quality characteristics of TE constructs such as ECM quantity and homogeneity, facilitating the gradual transformation of ‘TE constructs’ in well characterized ‘TE products’.

Introduction

As the field of tissue engineering (TE) matures, the need for novel techniques to characterize engineered constructs (i.e. cells/tissue combined with scaffolds) in a more insightful and quantitative manner becomes imperative. Currently, standard techniques such as histological sectioning and Live/Dead viability/cytotoxicity staining show limited potential as quality controls for TE constructs as these techniques only allow assessment of tissue distribution in two dimensions, with loss of information and with limited depth resolution while being destructive in nature. (1-4) Techniques such as confocal microscopy may offer a potential for three dimensional (3D) visualization, however again a limited depth resolution (~300 μm) hinders their performance when larger TE construct need to be analyzed. (5)

Recent advances in 3D imaging techniques and image analysis strategies have demonstrated the potential of addressing some of the shortfalls of these currently applied methods for accurate TE construct analysis. In particular X-ray microfocus computed tomography (microCT) has been frequently applied as a 3D quantitative imaging technique to assess scaffold structure, (6-8) as well as bone ingrowth after *in vivo* implantation. (6, 9-14) Furthermore it has been employed for time-lapsed follow-up of mineralization inside scaffolds during *in vitro* static (15-17) or bioreactor cultures. (13, 18, 19) In most of these studies polymeric, ceramic, collagen scaffolds or composites were used, in which mineralized extracellular matrix (ECM) could be separated from the scaffold for the purpose of volume calculations and no significant material-dependent artifacts were present. However, when imaging ECM or tissue growth in metallic scaffolds or around implants, additional caution has to be taken during image analysis as metal artifacts (20, 21) can significantly influence the accuracy of the quantification of the newly formed ECM or tissue volume. (22, 23)

Several studies have shown that when using phase contrast imaging, in most cases only available by synchrotron radiation, non-mineralized ECM formed *in vitro* in 3D TE constructs can be visualized. (24-26) However, routine access to systems allowing phase

contrast imaging is limited and there are restrictions on the sample specifications. On the other hand, by using the more routinely available desktop microCT in standard absorption mode, without the use of a contrast agent, it has not been possible yet to visualize *in vitro* produced non-mineralized ECM in 3D scaffolds. (24, 27) To address this limitation osmium tetroxide, (28) a well-known X-ray opaque staining, has been used to visualize cells in 3D constructs. This stain is however toxic to cells, thus cannot be used for non-invasive quality control of ECM growth in the TE construct.

In this study, we propose contrast enhanced nanofocus CT (CE-nanoCT), (29) as a 3D imaging technique that combines the high spatial and contrast resolution of nanoCT with the use of contrast agents, to characterize engineered ECM in TE constructs after *in vitro* culture. In particular we performed a 3D quantitative and qualitative structural and spatial assessment of the *in vitro* engineered ECM, formed during static and bioreactor cell culturing in titanium alloy scaffolds. By using metallic scaffolds in this case study we additionally proved the effectiveness of CE-nanoCT, as these scaffold types represent the worst case scenario with regard to material-dependent image artifacts. The two selected tissue-specific contrast agents that were used to stain the TE construct after culture were Hexabrix[®] and phosphotungstic acid (PTA). The latter is known to bind to connective tissues, and more specifically to collagen and fibrin. (30) The former contains a negatively charged ioxaglate, which will be locally repulsed by the negative fixed charge density of the tissue, thus all tissues which do not contain a negative charge will be stained. (31, 32) Additionally, Hexabrix[®] has been used for *in vivo* animal studies (33) and in a clinical setting, (34) and thus is a potential candidate for non-invasive TE construct quality assessment. To evaluate the potential of CE-nanoCT for 3D visualization and quantification of *in vitro* engineered ECM by culture of human periosteum derived cells (hPDCS, i.e. a cell type that has been seen to be multipotent and to contribute in bone regeneration (35, 36)) in 3D titanium alloy scaffolds, a comparison was

made to routine physical measurement techniques, such as Live/Dead viability/cytotoxicity for cell viability, picrosirius red staining for collagen content and ECM weight measurements.

Materials and Methods

Ti6Al4V scaffolds

3D additive manufactured open porous Ti6Al4V scaffolds (subsequently referred to as Ti scaffolds: $\varnothing = 6$ mm, $h = 6$ mm, porosity = $73 \pm 1\%$, strut diameter = 245 ± 2 μm and pore size = 755 ± 3 μm), produced on an in-house developed selective laser melting (SLM) machine, (37) were used. The design was based on a parametric unit cell (FIG. 1A), which consists entirely of identical beams with constant circular cross-section (0.1 mm) and a beam length of 0.9 mm. Figure 1B visualizes a produced open porous Ti scaffold. Prior to cell seeding, all scaffolds were pre-wetted by vacuum impregnation in cell culture medium for 2 h in a humidified incubator at 37°C, and dried overnight in a non-humidified incubator. (38)

Standard 2D hPDC Culture

hPDCs were isolated from periosteal biopsies of different donors as described previously. (39) This procedure was approved by the ethics committee for Human Medical Research (KU Leuven) and with patient informed consent. hPDCs were expanded in Dulbecco's modified Eagle's medium with high-glucose (Invitrogen) containing 10% fetal bovine serum (BioWhittaker) and 1% antibiotic–antimycotic (100 units/mL penicillin, 100mg/mL streptomycin, and 0.25mg/mL amphotericin B; Invitrogen). The seeding density used for the two dimensional (2D) culture dish hPDC expansion was 6000 cells/cm². hPDCs were passaged at 80% – 90% confluency. At the time of experiment, cells (with a population doubling number of 15) were trypsinized with Tryple Express (Invitrogen) to be seeded on the scaffolds.

Static & bioreactor TE construct culture

A validated static seeding protocol was used for seeding 2D cultured hPDCs (cell seeding density 30000 cells/cm²) onto the preconditioned Ti scaffolds with an average cell seeding efficiency of 60%. (38) *In vitro* cell culture in the TE constructs lasted for 14, 21 and 28 days under static (n = 7) or dynamic (n = 7) culture conditions. For static culture, TE constructs were positioned in 12-well plates (Greiner Bio One) containing 3ml cell culture medium, and incubated at 37°C in a humidified and CO₂-controlled incubator (relative humidity: 95%, 5% CO₂). For bioreactor culture, TE constructs were cultured in an in-house developed perfusion bioreactor equipped with 7 parallel perfusion circuits (FIG. 1C). Each perfusion chamber, holding a single scaffold, was connected to an individual medium reservoir (disposable 50 ml Falcon tubes, BD Biosciences) containing 10 ml of cell culture medium via a Tygon[®] (Cole Parmer) tubing and via a two-stop tubing (BPT, Cole Parmer) connected to a peristaltic pump (IPC-24, Ismatec SA). Two different perfusion flow rates were used for the bioreactor culture: the low flow rate used was 0.04 ml/min while the high flow rate was 4 ml/min. In both static and bioreactor cultures medium was refreshed every two days for the entire culture duration.

CE-nanoCT

After static or dynamic culture the TE constructs were rinsed with 1ml phosphate buffered saline (PBS) and transferred to a 4% paraformaldehyde solution (Sigma) for 2 hours to fixate the ECM. The TE constructs were stored in PBS prior to analysis. Two contrast agents were used as received, namely Hexabrix[®] 320 (Guerbet Nederland B.V) and PTA (VWR International). During preliminary experiments (data not shown), for both contrast agents an exposure time of 30 min to consistently stain the entire TE constructs was selected.

Hexabrix[®] is a radio-opaque injectable solution containing ioxaglate meglumine (39.3 %) and ioxaglate sodium (19.6 %). Ioxaglate is a negatively charged ionic iodinated dimer that is locally repulsed by the negative fixed charge density of the ECM. As a

consequence, all tissues with a net negative charge will not be stained, while Hexabrix[®] will adsorb to the rest. All samples were, before imaging, immersed in a solution of Hexabrix[®] 320 (20% in PBS), then wrapped in parafilm and stably positioned in the nanoCT system for imaging.

PTA is a soft tissue contrast agent containing tungsten, which confers strong X-ray contrast when attached to biological tissue, and has a strong binding affinity to fibrin and collagen. Hence PTA is a very useful contrast agent to specifically visualize the collagen and fibrin content in ECM. Similar to Hexabrix[®], all samples were, prior to imaging, immersed in a solution of PTA (1.25g/50ml PBS), were then wrapped in parafilm and were stably positioned in the nanoCT system.

The nanoCT system employed in this study was a Phoenix NanoTom S (GE Measurement and Control Solutions) with a 180 kV/15 W high-performance nanofocus X-ray tube. It was equipped with a tungsten target and was operated, for all scans, at a voltage of 90 kV and a current of 170 μ A. A 1 mm aluminum and 1 mm copper filter was used to reduce beam hardening and metal artifacts as much as possible. The exposure time was 500 ms and a frame averaging of 1 and image skip of 0 was applied, resulting in a total scanning time of 20 minutes per TE construct. The scanning time was kept low to avoid sample drying during scanning, to allow routine screening and to enable in future more non-invasive use and real-time monitoring. The reconstructed images had an isotropic voxel size of 3.75 μ m.

3D visualization, and image processing and analysis

For 3D visualization of the TE constructs, CTVox (Bruker micro-CT) was used. For image processing and quantification of the ECM volume in the TE constructs we used CTAn (Bruker micro-CT) according to the scheme in FIG. 2. At first the reconstructed dataset of the entire TE construct was fragmented in different subsets with a similar amount of metallic artifacts (step 1). By using a 3-level automatic Otsu segmentation algorithm (40) on the

individual 2D slices, the ECM was separated from both the scaffold and the background, the latter including noise and metal artifacts (step 2). As a result, grey-scale images with distinct grey-scale values for scaffold, ECM and background were generated for the different subsets. A global threshold was then chosen manually to select the ECM (step 3). In order to reduce the errors introduced by the partial volume effect and metallic artifacts for analyzing the ECM volume, the binarized images for the Ti structure were dilated by 2 voxels and subtracted from the dataset of binarized ECM images (step 4). The noise was minimized by removing black speckle noise smaller than 500 voxels and white speckle noise smaller than 2000 voxels. In order to solidify the resulting structure, a 'closing' operation (~ 2 voxels) was performed on the resulting images (step 4), providing images suitable for the 3D analysis of the ECM volume. Finally, the ECM volume in the TE constructs was analyzed by performing a 3D analysis on the binarized and processed images (step 5).

Physical characterization of TE constructs for comparison to the CE-nanoCT data

In order to gain further understanding on the properties of the cultured TE constructs, subsequent experimental analyses were performed, as described in this section. They were also used to evaluate the potential of CE-nanoCT and assess the levels of complementarity between established analyses and the suggested imaging technique.

Cell viability by Live/Dead viability/cytotoxicity staining

The cell viability in the TE constructs was evaluated using Live-Dead viability/cytotoxicity staining (Invitrogen, USA). Constructs were rinsed with 1ml PBS, incubated in the staining solution (0.5 μ l Calcein AM and 2 μ l Ethidium Homodimer in 1ml PBS) for 20 min under normal cell culture conditions and finally imaged using a Leica M165 FC microscope (38).

Collagen content by picrosirius red staining

The collagen-containing ECM production on the TE constructs was characterized by picosirius red staining (1mg/mL Sirius Red in saturated Picric acid). (41) The stained samples were thoroughly washed with distilled water to remove unbound dye and dried at 37°C before qualitative analysis by stereomicroscopy. For quantitative analysis, the picosirius red dye was dissolved in 0.2M NaOH/Methanol (1:1 ratio) with mild shaking overnight, and the optical density was measured at 492nm using a microplate reader (TECAN) for 1 ml triplicate samples for each condition.

ECM weight measurement

The liquid in the TE constructs was carefully removed using vacuum after which they were dried overnight in 37°C and subsequently weighed on a high accuracy balance (Sartorius CPA225D). Ti scaffolds were cleansed ultrasonically, immersed for 10 min in acetone, 10 min in ethanol 70%, and 10 min in distilled water, subsequently an alkali treatment was applied for 24 h at 60°C in a 5 M sodium hydroxide (Sigma-Aldrich) solution, samples were rinsed with distilled water, and finally sterilized in a steam autoclave. The weight of the cleansed Ti scaffold was subtracted from the total weight, resulting in the net ECM weight.

Results

CE-nanoCT allows 3D visualization of ECM in TE constructs

As a first step in this study TE constructs were scanned with nanoCT without the use of contrast agents. It allowed a visual inspection of 3D hPDC-driven ECM formation in the TE constructs after static or dynamic *in vitro* culture. However the reconstructed 2D slices (FIG. 3A) were of low image quality (i.e. low contrast between ECM and background) making accurate qualitative evaluation and further 3D quantification impossible. When using Hexabrix[®] and PTA, both contrast agents respectively infiltrated and bonded to the ECM, resulting in an increase in 3D grey-scale intensity of the ECM for static (FIG. 3B) as well as

for both (low and high flow rate) bioreactor culture derived TE constructs (FIGs. 3C and 3D). Black arrows in the image indicate ECM boundaries within the TE construct. The high contrast difference between ECM, background and Ti scaffold allowed further processing of the raw CE-nanoCT images.

Live/dead viability/cytotoxicity staining was employed as a benchmark analysis of cell viability and distribution on the different TE constructs. The fluorescent images showed that cells were distributed over the entire outer TE construct surface, indicating similar results for all 3 culture conditions (FIG. 4A). However CE-nanoCT images of the same TE constructs showed that for static culture, ECM was only formed at the scaffold periphery, resulting in only partially ECM filled TE constructs, while in the bioreactor cultured TE constructs ECM was also found back throughout the internal TE construct volume (FIG. 4B).

The cross-sectional CE-nanoCT images were subsequently binarized and processed as described in FIG. 2 to quantify the volume of the ECM formed. FIG. 4C shows representative binarized images for all culture conditions, visualizing the ECM in white and background plus Ti scaffold in black. In the case of static culture only thin strands of ECM were present at the periphery of the TE construct, resulting in a loss of representation after binarization and correction for metallic artifacts (i.e. step 4 in FIG. 2), making the 3D quantification and visualization of the ECM in statically cultured TE constructs inaccurate. Qualitative assessment of the spatial ECM distribution in 3D in these samples was nevertheless possible throughout the entire TE construct.

CE-nanoCT allows 3D quantification of ECM volume in TE constructs

Image analysis of the binarized CE-nanoCT slices for the different contrast agents allowed to quantify the total amount of stained ECM formed within the available void volume (i.e. total TE construct volume excluding the volume of Ti scaffold) for the bioreactor perfusion culture conditions, which was not possible for statically cultured TE constructs as

the amount of ECM formed was too small to be quantified. In order to comprehend the CE-nanoCT-based ECM characterization in the TE constructs, a comparison was made to two established methods for ECM assessment, namely picosirius red staining to measure the collagen content and ECM dry weight measurement (FIG. 5 and FIG. 6). TE constructs giving increased values of picosirius red values (absorption at 492nm, FIG. 5A) also showed increased values of ECM when measured via Hexabrix[®] and PTA stained CE-nanoCT (FIG 5B). Overall, Hexabrix[®] stained CE-nanoCT values were seen to follow the picosirius red absorption values more closely than the PTA stained ones with a stronger dependency on the flow rate used for TE construct culture. The ECM volume after Hexabrix[®] staining was seen to fit linearly with net dry weight values independent from the flow rate used (FIG. 6A). While for TE constructs cultured at high flow rate, only a small difference in ECM volume was observed between the Hexabrix[®] and PTA staining, for those TE constructs cultured at a low flow rate, Hexabrix[®] staining resulted in significantly higher ECM volumes than those obtained via PTA staining (FIG. 5B) because of the binding specificity of PTA to proteins and collagen. Indeed, both FIGs 5B and 6B show that a part of the ECM was not stained by PTA, and that this part was more pronounced for the lower ECM content conditions (seen for the low flow rate).

CE-nanoCT allows spatial visualization and quantification of the ECM in TE constructs

FIGs 7B and 7C show typical 3D renderings of the CE-nanoCT images (both for Hexabrix[®] and PTA staining respectively) for a bioreactor perfusion cultured TE construct at high flow rate, together with the corresponding Live/Dead viability/cytotoxicity staining (FIG. 7A) and picosirius red staining (FIG. 7D). The 3D image obtained with Hexabrix[®] staining, visualizing all the ECM present in the construct in green, showed a comparable ECM distribution as the Live/Dead viability/cytotoxicity staining for the outer TE construct surface (indicated by the white arrows). The PTA stained 3D images, showing the collagen

and fibrin containing ECM in red, had a comparable ECM distribution as the picosirius red staining for the outer TE construct surfaces. Moreover, the 3D rendered CE-nanoCT images of both the Hexabrix[®] and PTA staining allowed a full 3D visualization of the ECM distribution throughout the entire TE construct (supplementary videos may be seen in the appendix). A volumetric ECM distribution histogram over the TE construct height was plotted both for the Hexabrix[®] and PTA staining (FIG. 8), giving an indicative example of the 3D qualitative (distribution) and quantitative (volume of ECM) information obtainable with CE-nanoCT. Although a homogeneous ECM distribution over the TE construct height could be expected, both stainings showed that a larger amount of ECM was formed at the bottom of the TE construct.

Discussion

In order to successfully implement TE constructs as part of a clinical therapy, it is necessary to develop quality control tools that will ensure accurate and consistent TE construct release specifications. (42) In general a substantial amount of routine lab techniques currently used in TE were initially developed and optimized for 2D analysis of cell growth, distribution and matrix secretion in culture flasks and not for use in a 3D setting such as TE constructs (Table 1). For example the information obtained by destructive scanning electron microscopy (SEM) remains 2D and rather elusive even when multiple sample slices are analyzed. (8, 25, 27) Thus one has to be careful when using 2D validated techniques to draw 3D conclusions. Proper validation under 3D conditions and/or complementary use of additional real 3D information requires substantial additional research, but it is a much safer route to obtain reliable information of 3D cell and tissue behavior. Hence advanced 3D methods to, preferably non-invasively, monitor TE construct properties need to be further developed.

X-ray micro and nanoCT offer a potential solution because of their non-destructive 3D character. However, the value of X-ray CT-based information for TE will ultimately be a trade-off of factors such as physicochemical, morphological and dimensional TE construct properties, contrast enhanced agent and equipment limitations (Table 2). According to specific study objectives, a customized strategy will be required to extract the necessary information in a robust way, ranging from (i) accurate and detailed (100s of μm scale) identification and quantification of different TE construct components limited to small TE construct samples and using phase contrast imaging, (25) to (ii) using standard desktop micro- or nanoCT as a routine 3D imaging technique for whole TE construct analysis (mm to cm scale) and quantification of mineralization after *in vivo* implantation. (10, 13) The latter approach, without the use of a contrast agent, has also been used for static or bioreactor *in vitro* cultures, (16, 18, 19) showing distinct contrast differences between mineralized matrix and scaffold. Phase contrast imaging (24-26) or microCT combined with osmium tetroxide as a contrast agent (28) have shown their potential to assess non-mineralized ECM in an *in vitro* engineered TE construct. However, the limited availability of synchrotron radiation or CT systems allowing phase contrast imaging, the toxicity of osmium tetroxide and the high cost associated with its disposal, all hamper their use as routine quality control for TE constructs.

Both contrast agents used in this work (Hexabrix[®] and PTA) increased the grey-scale intensity difference between the different phases in the TE constructs as seen in FIG 3. In the static culture case, ECM was only found around the periphery of the Ti scaffold in contrast with ECM the bioreactor cultured TE constructs. Porter *et al.* (18) also reported peripheral deposition of mineralized matrix on statically cultured TE constructs in respect to a more dense and spatially homogeneous distribution of mineralized matrix in bioreactor cultured TE constructs based on microCT analysis. Additionally they also reported that mineralized matrix formation was initiated at the scaffold periphery and progressed towards the scaffold center

over a period of 44 days. These dynamics may be attributed to fluid flow and convective nutrient and oxygen transport throughout the TE construct volume during culture. (43-45) In this study CE-nanoCT revealed a dramatic increase of ECM content for bioreactor cultured TE constructs (up to 75% of void volume) with respect to the statically cultured ones (less than 4% of void volume). The low ECM quantity in the static culture case was below the CE-nanoCT threshold for ECM quantification, which in this study was determined to be an ECM volume lower than 4% of the total Ti scaffold void volume (FIG. 4). This lower quantification limit was directly related to the artifacts introduced by the metallic scaffolds used in this work. (46) For other scaffold materials however, it is anticipated that the lower quantification threshold of CE-nanoCT will further decrease, since material-dependent artifacts will be reduced compared to the worst case scenario described here.

CE-nanoCT results were then compared to known physical ECM characterization methods, such as dry net weight as a global ECM related parameter and picrosirius red staining as a collagen specific assay, to comprehend the CE-nanoCT data and hence evaluate the potential of CE-nanoCT for 3D ECM quantification in TE constructs. In FIG. 6A, the relative ECM void volume filling obtained via Hexabrix® staining (an equilibrium contrast agent, thus it does not bind to the ECM) was correlated to the net dry weight, resulting in a linear correlation for both flow rates, suggesting that Hexabrix® stains most of the ECM in a quantitative manner. However when using the more tissue-specific contrast agent PTA, which is known to bind to various proteins and connective tissue, (47, 48) a difference with Hexabrix® staining was found (FIG. 5B), while when comparing to the net dry weight, it was shown that PTA only stained a fraction of the ECM (FIG. 6B).

FIG. 5 shows a qualitative relationship between experimental values obtained via the collagen specific picrosirius red staining and CE-nanoCT values demonstrating both increasing trends over time. Additionally, a clear flow rate dependence was seen (FIGs 5B)

for both PTA and Hexabrix® stains. It can be observed that TE constructs cultured under high flow rate showed a larger fraction of the ECM stained by PTA, which could be explained as an ECM richer in protein components (on which PTA may specifically bind). Fluid flow is known to enhance matrix synthesis within TE constructs during perfusion culture. (19, 44, 49) Furthermore differences in fibrillar collagen organization of the ECM, which are flow dependent, (50) could also explain the ECM differences that were observed by PTA staining as the ECM morphology could influence the binding mechanism of PTA to the ECM proteins. In FIG. 5, it may also be observed that the difference in collagen content, as determined by picosirius red staining, for the different flow rates is less pronounced than the one observed with the PTA staining. However one has to keep in mind that the picosirius red staining was used without any customization and validation for the specifics of the 3D environment under investigation, which could underestimate actual collagen content. (45) Certainly, for more dense TE constructs, like the ones obtained from high flow rate culture, this issue becomes more relevant due to increased inter-construct mass transport limitations that would affect the performance of the assay.

CE-nanoCT-based imaging and quantification clearly show that by using this technique information that could not be previously generated by standard experimental techniques such as microscopy of TE constructs stained with Live/Dead viability/cytotoxicity or collagen-specific picosirius red staining which are line-of-sight techniques lacking a 3D internal visualization potential may now be obtained. Hence, a direct validation of CE-nanoCT using these techniques is irrelevant. Images obtained by standard experimental techniques are mainly limited to surface restricted TE construct characterization as they are line-of-sight techniques and only provide limited depth information. (49, 51) Not taking into account the latter limitation may result in the misinterpretation of statically cultured TE constructs as being full of ECM while in reality only an outer layer of ECM exists, as

confirmed by CE-nanoCT (FIG. 4). A potential validation technique could be histological sectioning. However, the use of Ti scaffolds in this work does not allow the sectioning of the produced TE constructs, and thus will also not present full 3D data.

To conclude, for the combination of factors used in this work, i.e. scaffold size and material type, type of CT device and scanning mode (Table 2), and its objective, CE-nanoCT has shown potential as a cost effective TE construct quality control methodology, by providing volumetric and distribution measurements throughout the entire TE construct (FIGs 7 and 8). Although there are preliminary indications for ECM composition analysis via this method which need to be further investigated, the novel information that CE-nanoCT generates will assist to increase our insight in the ECM characteristics within *in vitro* manufactured TE constructs. In this study we showed proof of concept for CE-nanoCT as a ‘whole-construct’ imaging technique with non-invasive potential that enables 3D visualization and quantification of *in vitro* engineered ECM in TE constructs. The development of robust tools and methodologies such as CE-nanoCT to assess important and potentially critical quality characteristics of TE constructs such as ECM quantity and homogeneity, can facilitate the gradual transformation of ‘TE constructs’ to well characterized ‘TE products’.

Acknowledgements

IP is funded by the ENDEAVOUR project G.0982.11N of the Research Foundation Flanders (FWO Vlaanderen). MS is supported by a Ph.D. grant of the Agency for Innovation by Science and Technology (IWT/ 111457). GK and LG acknowledge support by the European Research Council under the European Union's Seventh Framework Program (FP7/2007-2013)/ERC grant agreement n°279100. This work is part of Prometheus, the Leuven Research & Development Division of Skeletal Tissue Engineering of the KU Leuven: www.kuleuven.be/prometheus.

References

1. Eniwumide JO, Yuan H, Cartmell SH, Meijer GJ, de Bruijn JD. Ectopic bone formation in bone marrow stem cell seeded calcium phosphate scaffolds as compared to autograft and (cell seeded) allograft. *Eur Cell Mater.*14:30-8; discussion 9. 2007.
2. Hedberg EL, Kroese-Deutman HC, Shih CK, Lemoine JJ, Liebschner MAK, Miller MJ, et al. Methods: A comparative analysis of radiography, microcomputed tomography, and histology for bone tissue engineering. *Tissue Engineering.*11:1356-67. 2005.
3. Stephens JS, Cooper JA, Phelan FR, Dunkers JP. Perfusion flow bioreactor for 3D in situ imaging: Investigating cell/biomaterials interactions. *Biotechnol Bioeng.*97:952-61. 2007.
4. Smith LE, Smallwood R, Macneil S. A comparison of imaging methodologies for 3D tissue engineering. *Microscopy research and technique.*73:1123-33. 2010.
5. Georgakoudi I, Rice WL, Hronik-Tupaj M, Kaplan DL. Optical Spectroscopy and Imaging for the Noninvasive Evaluation of Engineered Tissues. *Tissue Eng Part B-Re.*14:321-40. 2008.
6. van Lenthe GH, Hagenmuller H, Bohner M, Hollister SJ, Meinel L, Muller R. Nondestructive micro-computed tomography for biological imaging and quantification of scaffold-bone interaction in vivo. *Biomaterials.*28:2479-90. 2007.
7. Jungreuthmayer C, Donahue SW, Jaasma MJ, Al-Munajjed AA, Zanghellini J, Kelly DJ, et al. A Comparative Study of Shear Stresses in Collagen-Glycosaminoglycan and Calcium Phosphate Scaffolds in Bone Tissue-Engineering Bioreactors. *Tissue Eng Pt A.*15:1141-9. 2009.

8. Peyrin F, Mastrogiacomo M, Cancedda R, Martinetti R. SEM and 3D synchrotron radiation micro-tomography in the study of bioceramic scaffolds for tissue-engineering applications. *Biotechnol Bioeng.*97:638-48. 2007.
9. Jones AC, Arns CH, Hutmacher DW, Milthorpe BK, Sheppard AP, Knackstedt MA. The correlation of pore morphology, interconnectivity and physical properties of 3D ceramic scaffolds with bone ingrowth. *Biomaterials.*30:1440-51. 2009.
10. Jones AC, Arns CH, Sheppard AP, Hutmacher DW, Milthorpe BK, Knackstedt MA. Assessment of bone ingrowth into porous biomaterials using MICRO-CT. *Biomaterials.*28:2491-504. 2007.
11. Cancedda R, Cedola A, Giuliani A, Komlev V, Lagomarsino S, Mastrogiacomo M, et al. Bulk and interface investigations of scaffolds and tissue-engineered bones by X-ray microtomography and X-ray microdiffraction. *Biomaterials.*28:2505-24. 2007.
12. Papadimitropoulos A, Mastrogiacomo M, Peyrin F, Molinari E, Komlev VS, Rustichelli F, et al. Kinetics of in vivo bone deposition by bone marrow stromal cells within a resorbable porous calcium phosphate scaffold: An X-ray computed microtomography study. *Biotechnol Bioeng.*98:271-81. 2007.
13. Guldberg RE, Duvall CL, Peister A, Oest ME, Lin ASP, Palmer AW, et al. 3D imaging of tissue integration with porous biomaterials. *Biomaterials.*29:3757-61. 2008.
14. Chai YC, Kerckhofs G, Roberts SJ, Van Bael S, Schepers E, Vleugels J, et al. Ectopic bone formation by 3D porous calcium phosphate-Ti6Al4V hybrids produced by perfusion electrodeposition. *Biomaterials.*33:4044-58. 2012.

15. Hagenmueller H, Hofmann S, Kohler T, Merkle HP, Kaplan DL, Vunjak-Novakovic G, et al. Non-invasive time-lapsed monitoring and quantification of engineered bone-like tissue. *Annals of Biomedical Engineering*.35:1657-67. 2007.
16. Cartmell S, Huynh K, Lin A, Nagaraja S, Guldborg R. Quantitative microcomputed tomography analysis of mineralization within three-dimensional scaffolds in vitro. *J Biomed Mater Res Part A*.69A:97-104. 2004.
17. Frohlich M, Grayson WL, Marolt D, Gimble JM, Kregar-Velikonja N, Vunjak-Novakovic G. Bone Grafts Engineered from Human Adipose-Derived Stem Cells in Perfusion Bioreactor Culture. *Tissue Eng Pt A*.16:179-89. 2010.
18. Porter BD, Lin ASP, Peister A, Hutmacher D, Guldborg RE. Noninvasive image analysis of 3D construct mineralization in a perfusion bioreactor. *Biomaterials*.28:2525-33. 2007.
19. Hagenmuller H, Hitz M, Merkle HP, Meinel L, Muller R. Design and validation of a novel bioreactor principle to combine online micro-computed tomography monitoring and mechanical loading in bone tissue engineering. *Rev Sci Instrum*.81:014303. 2010.
20. De Man B, Nuyts J, Dupont P, Marchal G, Suetens P. Metal streak artifacts in X-ray computed tomography: A simulation study. *Ieee Transactions on Nuclear Science*.46:691-6. 1999.
21. Kerckhofs G, Schrooten J, Van Cleynenbreugel T, Lomov SV, Wevers M. Validation of x-ray microfocus computed tomography as an imaging tool for porous structures. *Rev Sci Instrum*.79:1-9. 2008.
22. Marechal M, Luyten F, Nijs J, Postnov A, Schepers E, van Steenberghe D. Histomorphometry and micro-computed tomography of bone augmentation under a titanium membrane. *Clin Oral Implan Res*.16:708-14. 2005.

23. Stoppie N, van der Waerden JP, Jansen JA, Duyck J, Wevers M, Naert IE. Validation of microfocus computed tomography in the evaluation of bone implant specimens. *Clinical Implant Dentistry and Related Research*.7:87-94. 2005.
24. Appel A, Anastasio MA, Brey EM. Potential for imaging engineered tissues with X-ray phase contrast. *Tissue Eng Part B Rev*.17:321-30. 2011.
25. Voronov RS, Vangordon SB, Shambaugh RL, Papavassiliou DV, Sikavitsas VI. 3D Tissue Engineered Construct Analysis via Conventional High Resolution MicroCT without X-Ray Contrast. *Tissue engineering Part C, Methods*. 2012.
26. Langer M, Liu Y, Tortelli F, Cloetens P, Cancedda R, Peyrin F. Regularized phase tomography enables study of mineralized and unmineralized tissue in porous bone scaffold. *Journal of microscopy*.238:230-9. 2010.
27. Albertini G, Giuliani A, Komlev V, Moroncini F, Pugnaroni A, Pennesi G, et al. Organization of extracellular matrix fibers within polyglycolic acid-polylactic acid scaffolds analyzed using X-ray synchrotron-radiation phase-contrast micro computed tomography. *Tissue Eng Part C Methods*.15:403-11. 2009.
28. Hilldore A, Wojtowicz A, Johnson AW. Micro-CT based quantification of non-mineralized tissue on cultured hydroxyapatite scaffolds. *J Biomed Mater Res Part A*.82A:1012-21. 2007.
29. Kerckhofs G, Sains, J., Wevers, M., Van de Putte, T., and Schrooten, J. Contrast-enhanced nanofocus computed tomography images the cartilage subtissue architecture in three dimensions. *European Cells and Materials*.accepted. 2013.
30. Metscher BD. MicroCT for comparative morphology: simple staining methods allow high-contrast 3D imaging of diverse non-mineralized animal tissues. *BMC physiology*.9:11. 2009.

31. Xie L, Lin ASP, Levenston ME, Guldberg RE. Quantitative assessment of articular cartilage morphology via EPIC- μ CT. *Osteoarthritis Cartilage*.17:313-20. 2009.
32. Palmer AW, Guldberg RE, Levenston ME. Analysis of cartilage matrix fixed charge density and three-dimensional morphology via contrast-enhanced microcomputed tomography. *Proceedings of the National Academy of Sciences of the United States of America*.103:19255-60. 2006.
33. Piscoer TM, Waarsing JH, Kops N, Pavljasevic P, Verhaar JAN, van Osch GJVM, et al. In vivo imaging of cartilage degeneration using [μ]CT-arthrography. *Osteoarthritis Cartilage*.16:1011-7. 2008.
34. Ginai AZ. Clinical Use of Hexabrix for Radiological Evaluation of Leakage from the Upper Gastrointestinal-Tract Based on Experimental-Study. *Brit J Radiol*.60:343-6. 1987.
35. Orwoll ES. Toward an expanded understanding of the role of the periosteum in skeletal health. *Journal of bone and mineral research : the official journal of the American Society for Bone and Mineral Research*.18:949-54. 2003.
36. De Bari C, Dell'Accio F, Luyten FP. Human periosteum-derived cells maintain phenotypic stability and chondrogenic potential throughout expansion regardless of donor age. *Arthritis and rheumatism*.44:85-95. 2001.
37. Van Bael S, Kerckhofs G, Moesen M, Pyka G, Schrooten J, Kruth JP. Micro-CT-based improvement of geometrical and mechanical controllability of selective laser melted Ti6Al4V porous structures. *Mat Sci Eng a-Struct*.528:7423-31. 2011.
38. Impens S, Chen YT, Mullens S, Luyten F, Schrooten J. Controlled Cell-Seeding Methodologies: A First Step Toward Clinically Relevant Bone Tissue Engineering Strategies. *Tissue Engineering Part C-Methods*.16:1575-83. 2010.

39. Eyckmans J, Luyten FP. Species specificity of ectopic bone formation using periosteum-derived mesenchymal progenitor cells. *Tissue Eng.*12:2203-13. 2006.
40. Otsu N. Threshold Selection Method from Gray-Level Histograms. *Ieee T Syst Man Cyb.*9:62-6. 1979.
41. Tullberg-Reinert H, Jundt G. In situ measurement of collagen synthesis by human bone cells with a sirius red-based colorimetric microassay: effects of transforming growth factor beta2 and ascorbic acid 2-phosphate. *Histochemistry and cell biology.*112:271-6. 1999.
42. Schneider CK, Salmikangas P, Jilka B, Flamion B, Todorova LR, Paphitou A, et al. Challenges with advanced therapy medicinal products and how to meet them. *Nat Rev Drug Discov.*9:195-201. 2010.
43. Grayson WL, Marolt D, Bhumiratana S, Frohlich M, Guo XE, Vunjak-Novakovic G. Optimizing the Medium Perfusion Rate in Bone Tissue Engineering Bioreactors. *Biotechnol Bioeng.*108:1159-70. 2011.
44. Bancroft GN, Sikavitsast VI, van den Dolder J, Sheffield TL, Ambrose CG, Jansen JA, et al. Fluid flow increases mineralized matrix deposition in 3D perfusion culture of marrow stromal osteoblasts in a dose-dependent manner. *Proceedings of the National Academy of Sciences of the United States of America.*99:12600-5. 2002.
45. Papantoniou I, Chai YC, Luyten FP, Schrooten J. Process quality engineering for bioreactor-driven manufacturing of tissue engineered constructs for bone regeneration. *Tissue Eng Part C Methods.* 2012.
46. Stradiotti P, Curti A, Castellazzi G, Zerbi A. Metal-related artifacts in instrumented spine. Techniques for reducing artifacts in CT and MRI: state of the art. *European spine journal : official publication of the European Spine Society, the*

European Spinal Deformity Society, and the European Section of the Cervical Spine Research Society.18 Suppl 1:102-8. 2009.

47. Hanker JS, Giammara BI. Principles and Techniques of Electron-Microscopy, Biological Applications, Vol 1, 2nd Edition - Hayat, Ma. Stain Technol.58:184-. 1983.

48. Blewitt PW. Histological and Histochemical Methods - Kiernan, Ja. Biochem Educ.12:46-. 1984.

49. Du DJ, Furukawa KS, Ushida T. 3D Culture of Osteoblast-Like Cells by Unidirectional or Oscillatory Flow for Bone Tissue Engineering. Biotechnol Bioeng.102:1670-8. 2009.

50. Pedersen JA, Lichter S, Swartz MA. Cells in 3D matrices under interstitial flow: Effects of extracellular matrix alignment on cell shear stress and drag forces. J Biomech.43:900-5. 2010.

51. Paletta JRJ, Mack F, Schenderlein H, Theisen C, Schmitt J, Wendorff JH, et al. Incorporation of Osteoblasts (Mg63) into 3d Nanofibre Matrices by Simultaneous Electrospinning and Spraying in Bone Tissue Engineering. Eur Cells Mater.21. 2011.

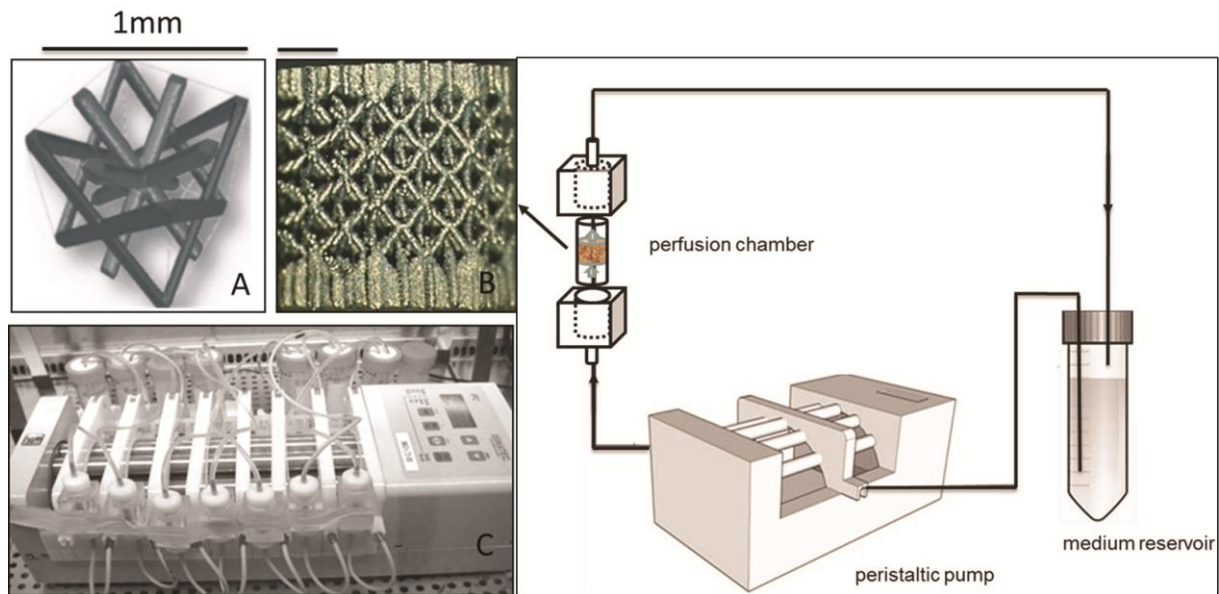


FIG. 1. (A) The parametric unit cell of the computer aided design of the porous Ti scaffolds, which consists entirely of identical beams with constant circular cross-section (0.1 mm) and a beam length of 0.9 mm, (B) a typical image of an SLM produced Ti scaffold and (C) an image of the in-house developed perfusion bioreactor equipped with parallel perfusion circuits, (D) Schematic of the bioreactor setup used for 3D dynamic culture, consisting of a medium reservoir containing 10 ml of medium, a peristaltic pump forcing culture medium through the porous scaffold that was positioned in the perfusion chamber.

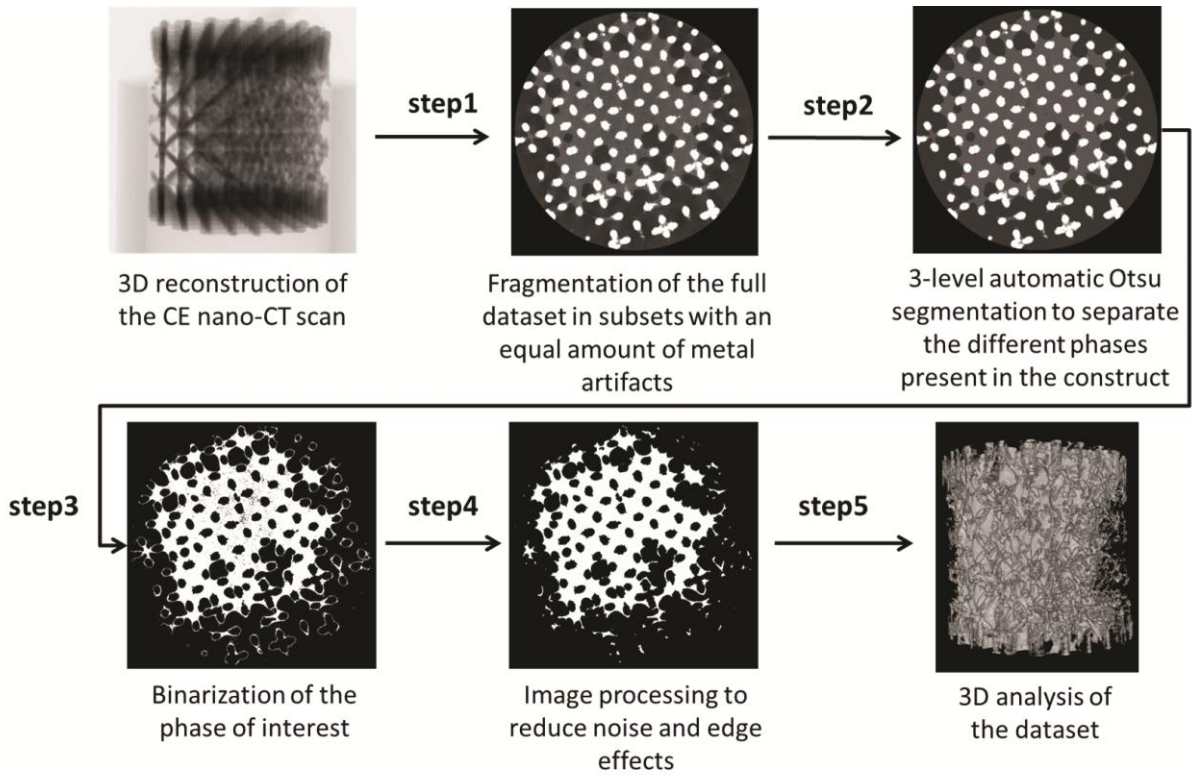


FIG. 2. Steps followed for image analysis from the 3D reconstruction of the CE-nanoCT scan to image processing and noise reduction to final 3D quantification and distribution analysis.

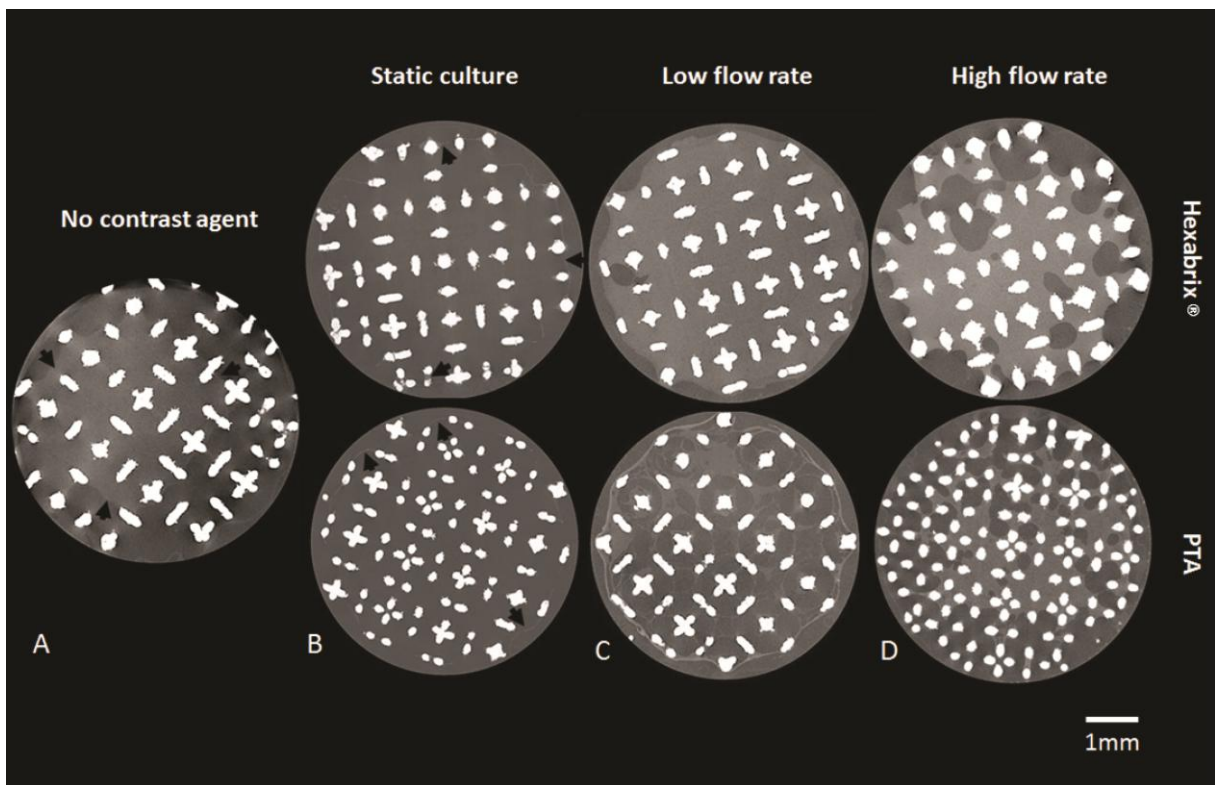


FIG. 3. Representative 2D CE-nanoCT cross-sections of a construct (A) scanned without

contrast agent, after bioreactor perfusion high flow rate (B) scanned after static culture with both Hexabrix[®] and PTA, (C) after bioreactor perfusion (low flowrate) culture with both Hexabrix[®] and PTA and (D) after bioreactor perfusion (high flowrate) culture with both Hexabrix[®] and PTA. Black arrows indicate boundaries of the ECM in the constructs.

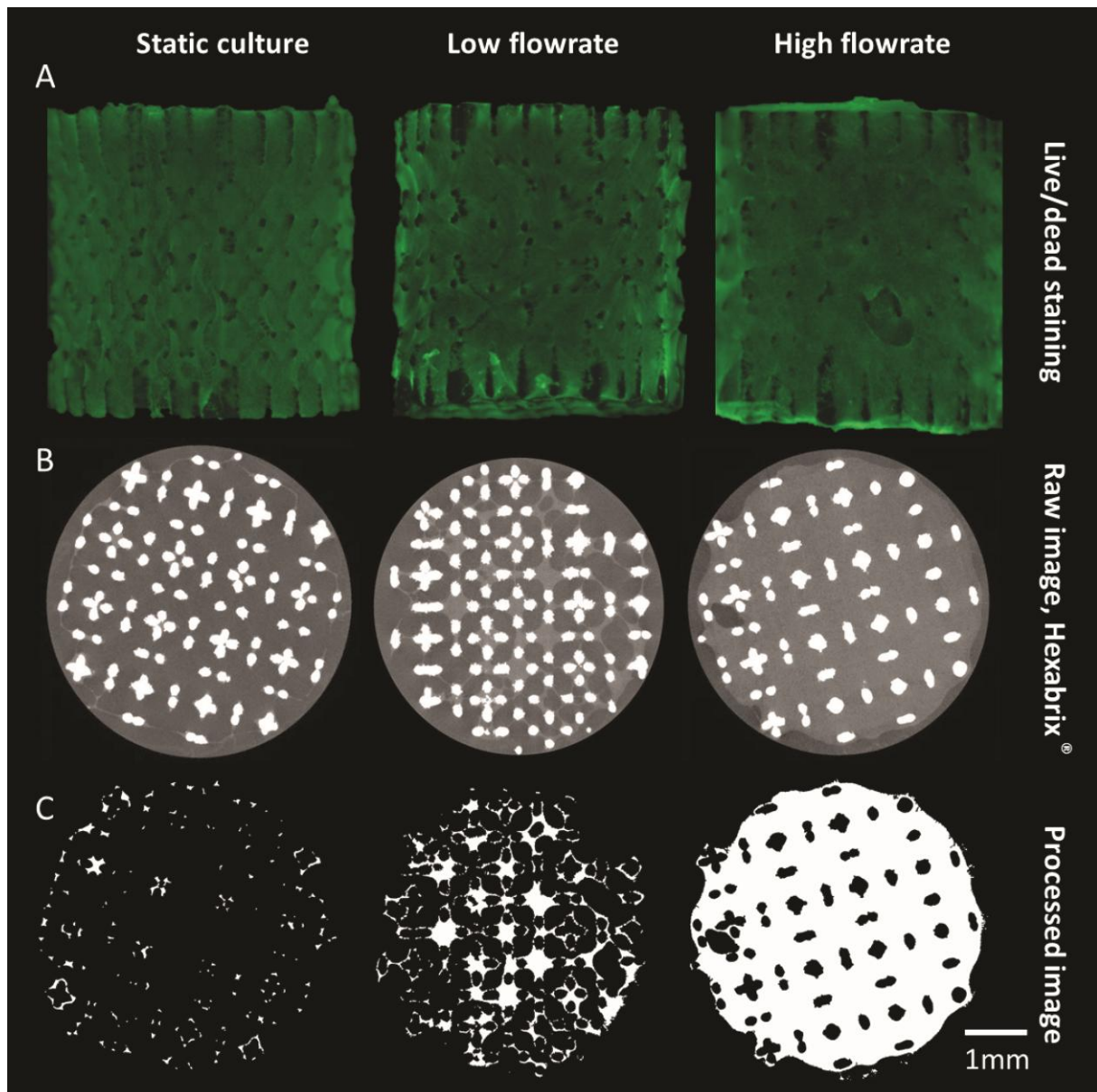


FIG. 4. (A) Live/dead viability/cytotoxicity staining of constructs cultured in different conditions, (B) typical 2D grey-scale CE-nanoCT cross-sections using Hexabrix[®] and (C) the corresponding binarized and processed cross-sections serving as input for the analysis of the ECM volume.

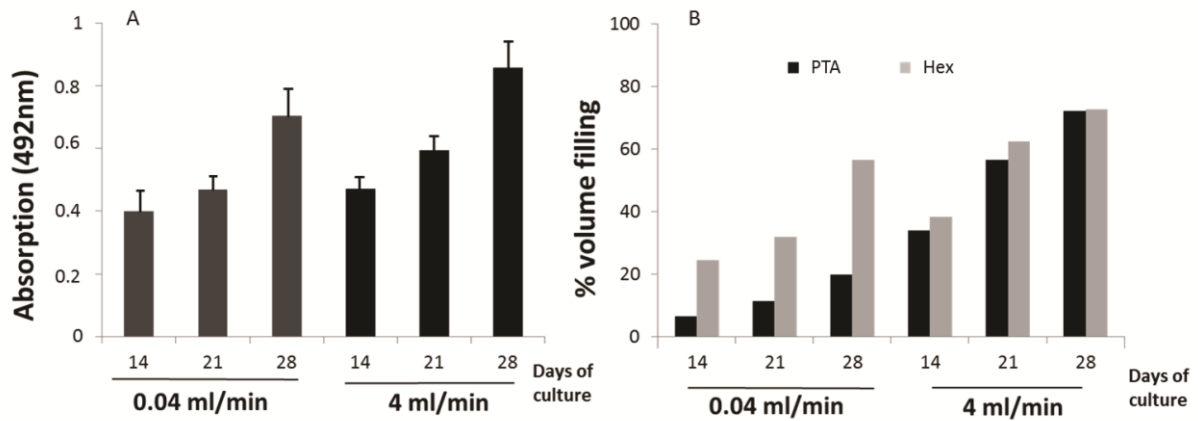


FIG. 5. (A) ECM content quantification via picosirius red for both flow rates over culture. (B) Relative ECM volume filling as function of the total TE construct internal void volume calculated based on CE-nanoCT using respectively Hexabrix® and PTA.

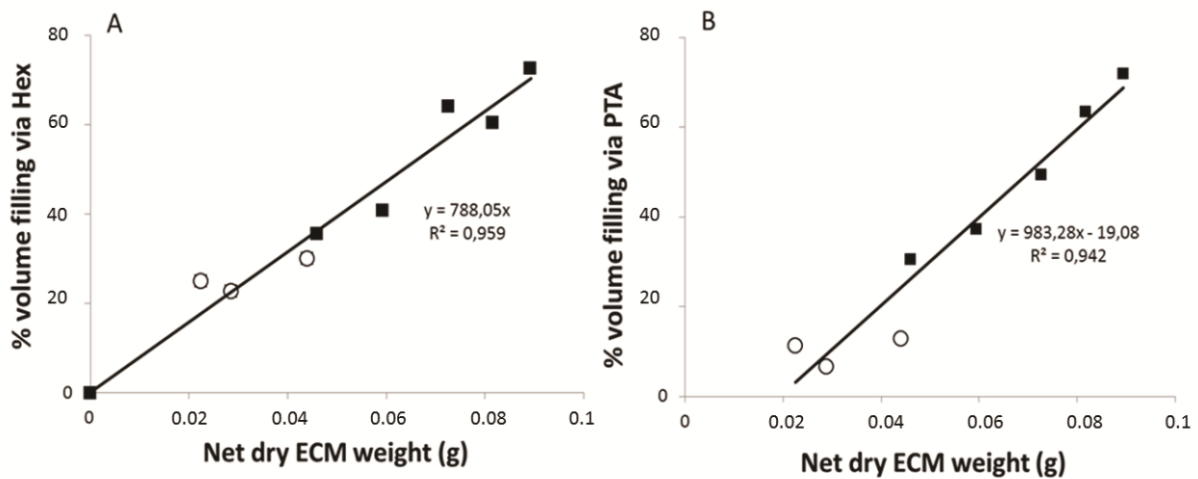


FIG. 6. Relative ECM volume filling as function of the total TE construct internal void volume calculated based on CE-nanoCT using respectively Hexabrix® (A) and PTA (B) in function of net dry weight. TE constructs were cultured under: (○) Low flow rate condition (0.04 ml/min); (■) High flow rate condition (4ml/min).

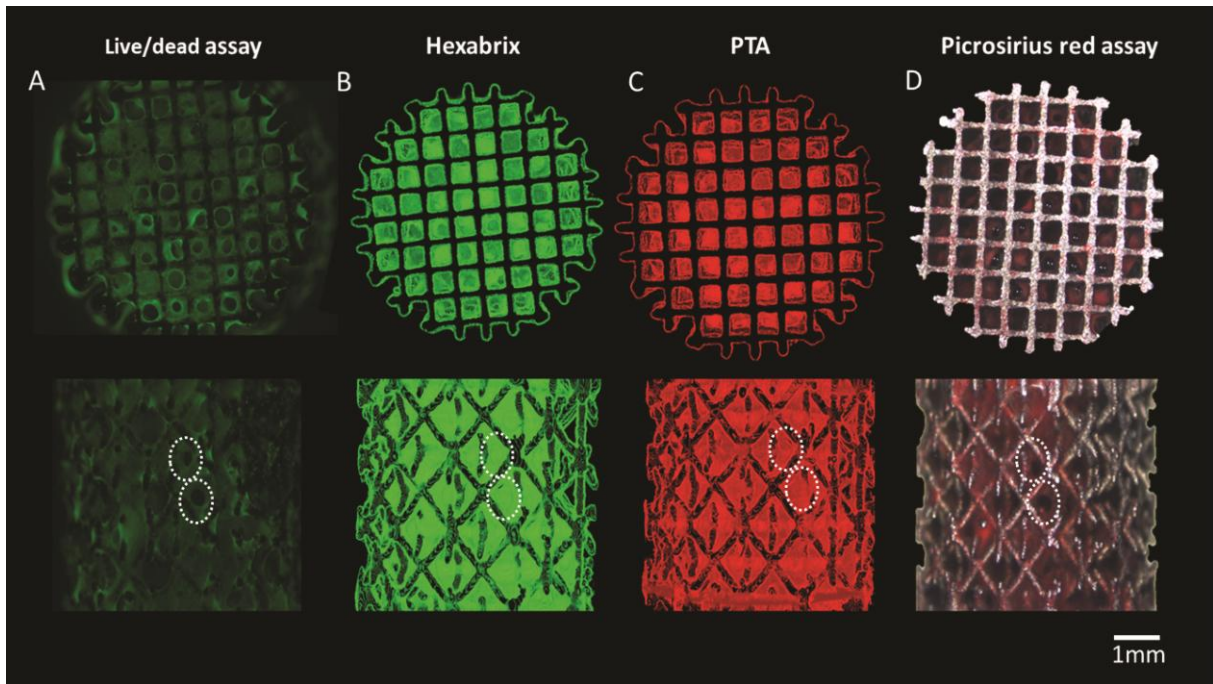


FIG. 7. Top and side view of the (A) live/dead staining of a perfusion bioreactor cultured construct at a flow rate of 4 ml/min, (B) 3D rendering of the CE-nanoCT images with Hexabrix® staining, (C) 3D rendering of the CE-nanoCT images with PTA staining and (D) Brightfield image of scaffold stained with Picro-sirius red. White dashed lines indicate identical geometric features of the ECM in microscopic images and reconstructed images.

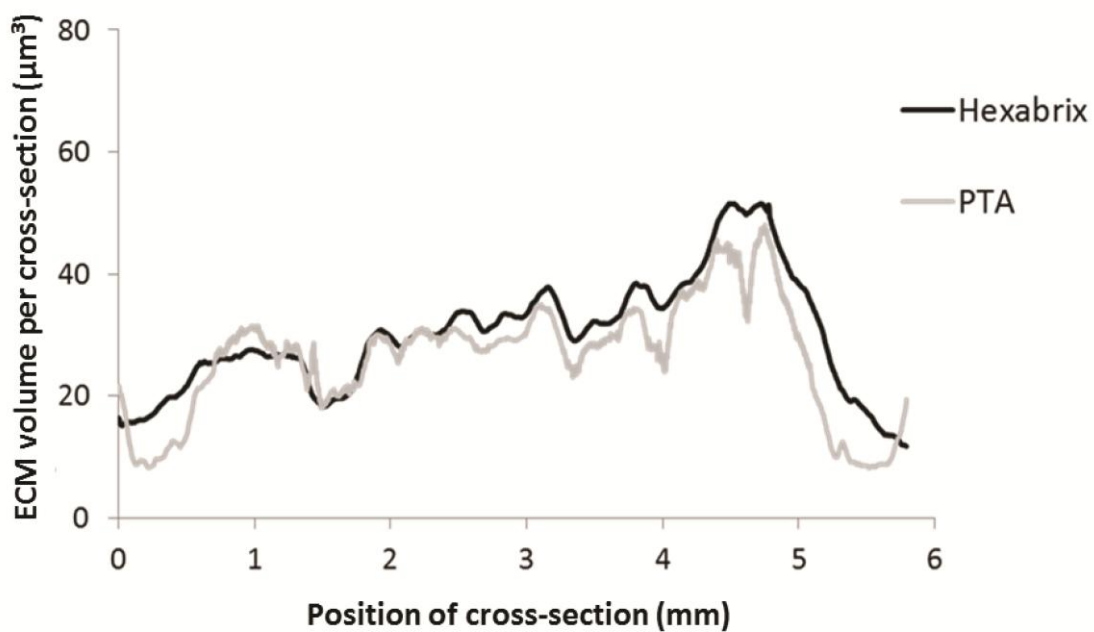


FIG. 8. Representative longitudinal ECM distribution throughout the full TE construct i.e.

volume of ECM per cross section, where the height of the section is 3.75 μm equal to the voxel size used for the analysis, in function of the scaffold height. Distributions obtained via Hexabrix[®] and PTA staining for a scaffold that was cultured for 21 days under a flow rate of 0.04 ml/min.

Routine Techniques	Specificity	Depth analysis	Scale	Ref.
Live/dead stain	cells	2D: limited depth	μm -mm	Du <i>et al.</i> ⁽⁴⁹⁾
Picro-sirius red stain	collagen	2D: limited depth	μm -mm	Paletta <i>et al.</i> ⁽⁵¹⁾
SEM and optical microscopy	cells, collagen, mineral phase	2D	$\sim \mu\text{m}$	Peyrin <i>et al.</i> ⁽⁸⁾
Alizarin red stain	Mineral phase	2D: limited depth	μm -mm	Frohlich <i>et al.</i> ⁽¹⁷⁾

Table 1: Categorization of bench imaging techniques that have been routinely employed for the visualization and analysis of 3D engineered tissues (related to bone TE).

	Specificity	Size Range	Resolution	Scaffold material	Imaging modality
CE-nanoCT	ECM and mineral phase (if present)	Whole construct (6 mm)	Micron scale	Titanium	Absorption - nanoCT

Voronov <i>et al.</i> ⁽²⁵⁾	cells, ECM, mineral phase,	Localized region in the samples (~500 µm)	Sub-micron scale	Poly-lactic acid (PLA)	Phase Contrast – micro-CT
Porter <i>et al.</i> ⁽¹⁸⁾	mineral phase	Whole construct (3 - 9 mm)	Micron scale	PCL	Absorption - micro-CT
Hilldore <i>et al.</i> ⁽²⁸⁾	ECM	Localized region in the samples	Micron scale	Hydroxy- apatite	Absorption - micro- CT
Albertini <i>et al.</i> ⁽²⁷⁾	ECM	Localized region in the samples	Sub-micron scale	PLLA/PGA	Phase contrast - synchrotron
Cartmell <i>et al.</i> ⁽¹⁶⁾	Mineral phase	Whole construct (6mm)	Micron scale	PLDL & Demineralized trabecular bone matrix scaffolds	Absorption - micro- CT
Langer <i>et al.</i> ⁽²⁶⁾	Mineral phase, ECM	Localized region in the samples	Micron scale	bone graft substitute	Phase contrast - synchrotron
Hagenmu	Mineral	Whole	Micron	Silkworm	Absorption

ller <i>et al</i> ⁽¹⁵⁾	phase	construct	scale	fibroin	n - micro- CT
-----------------------------------	-------	-----------	-------	---------	------------------

Table 2: Categorization and evaluation of X-ray tomography techniques employed for the visualization of features of *in vitro* 3D engineered tissues (related to bone TE).